Journal of Carcinogenesis
Covering Genesis to Therapeutics

Journal of Carcinogenesis, ISSN: 1477-3163
2024; Vol 23: Issue 1, https://carcinogenesis.com/

Development and Evaluation of Bioinspired Silver Nanoparticles (AgNPs) Synthesized Using Bacillus licheniformis for Wound Healing Applications.

Ms. Jayshri T. Swami[1], Dr. Nagoba Shivappa N[2*]

[1]Research Scholar, Centre for Research in Pharmaceutical Sciences (CRPS), Channabasweshwar Pharmacy College (Degree), Latur – 413512.

Email ID : swamijayashri520@gmail.com, https://orcid.org/0000-0002-1777-5940

[2]Professor and Head, Dept. of Pharmaceutics, Channabasweshwar Pharmacy College (Degree), Latur-413512, Dist. Latur. (MS).

Email ID : nagobashivraj@gmail.com, https://orcid.org/0000-0000-0001-7895-3088

***Corresponding Author:**

Dr. Nagoba Shivappa N.

Email ID : nagobashivraj@gmail.com

ABSTRACT

Background: Bioinspired nanotechnology offers a sustainable approach to developing advanced therapeutic systems with improved safety and efficacy. Bacillus licheniformis, a non-pathogenic microorganism, has emerged as an efficient biological platform for the eco-friendly synthesis of nanoparticles with biomedical potential.

Objective: This study aimed to develop, optimize, and characterize B. licheniformis–mediated silver nanoparticles (AgNPs) for wound healing applications using a Quality by Design (QbD) framework.

Methods: AgNPs were synthesized using bacterial supernatant and silver nitrate, with process parameters optimized via Central Composite Design (CCD). Physicochemical properties—including particle size, zeta potential, and entrapment efficiency—were evaluated using UV–Vis, FTIR, and SEM analyses. In vitro cytotoxicity, fibroblast migration (scratch assay), and antibacterial assays were conducted to assess biological performance.

Results: The optimized formulation (PF6) exhibited a mean particle size of 38.27 nm, zeta potential of −27.2 mV, and entrapment efficiency of 92.14%. UV–Vis and FTIR confirmed nanoparticle formation and bio-capping by microbial biomolecules, while SEM revealed spherical morphology. PF6 showed excellent stability across varied storage conditions and demonstrated dose-dependent cytocompatibility (IC_{50} = 35.63 µL/mL). Wound-healing assays revealed 58.5% fibroblast migration at 50 µg/mL, comparable to PDGF (67.8%). Moreover, PF6 exhibited notable antibacterial activity against E. coli (18.81 mm) and S. aureus (18.77 mm).

Conclusion: The study establishes B. licheniformis as a sustainable "green nanofactory" for synthesizing stable, biocompatible AgNPs with potent wound-healing and antimicrobial efficacy. These findings highlight the promise of microbial nanotechnology as a next-generation platform for regenerative medicine.

Keywords: *Bacillus licheniformis, bioinspired nanoparticles, silver nanoparticles, wound healing, QbD optimization, antibacterial activity*

How to Cite: Ms. Jayshri T. Swami, Dr. Nagoba Shivappa N, (2024) Development and Evaluation of Bioinspired Silver Nanoparticles (AgNPs) Synthesized Using Bacillus licheniformis for Wound Healing Applications. , *Journal of Carcinogenesis*, *Vol.23*, *No.1*, 138-151.

1. INTRODUCTION

The advancement of nanotechnology has opened new frontiers in modern drug delivery, particularly through the emergence of nanomedicine. Conventional drug delivery systems often encounter limitations such as poor solubility, rapid metabolism, a low therapeutic index, systemic toxicity, and the lack of site-specific action [1,2]. These challenges have spurred growing interest in bioinspired nanomedicine, which utilizes biological systems or natural processes for nanoparticle synthesis. Such approaches not only ensure superior biocompatibility and reduced toxicity but also offer sustainable, simple, and cost-effective alternatives to traditional chemical or physical synthesis methods [3–5].

Among various biological systems, microorganisms have emerged as promising candidates for nanomaterial synthesis. In

particular, *Bacillus licheniformis*, a non-pathogenic, Gram-positive bacterium, has gained considerable recognition as a "green nanofactory." This organism secretes enzymes, proteins, and metabolites that act as natural reducing and stabilizing agents, enabling the eco-friendly biosynthesis of nanoparticles without the need for hazardous chemicals. Nanostructures produced using *B. licheniformis* have been reported to be stable, biocompatible, and functionally versatile, making them highly suitable for drug delivery and biomedical applications [6,7].

Previous studies have demonstrated the versatility of this bacterium in producing various types of nanoparticles. For instance, *B. licheniformis* has been successfully employed for the extracellular synthesis of gold nanoparticles exhibiting uniform size, high stability, and potent antimicrobial properties. Similarly, this bacterium has been utilized for the biosynthesis of silver nanoparticles characterized by their strong antibacterial activity and nanoscale uniformity [8–10]. More recently, selenium nanoparticles synthesized using *B. licheniformis* have shown excellent antioxidant properties and high stability, with optimized fermentation processes achieving nearly complete conversion of precursor salts. Moreover, biopolymers such as levan obtained from this bacterium have been explored as excipients in colloidal drug delivery systems due to their ability to enhance stability and control drug release. Additionally, antimicrobial lipopeptides produced by *B. licheniformis* provide synergistic therapeutic benefits when incorporated into nanomedicine platforms [11,12].

Therefore, the present research focuses on the formulation and evaluation of bioinspired nanomedicine using *Bacillus licheniformis*. The study aims to develop a reliable, simple, and eco-friendly approach for synthesizing biocompatible nanocarriers. The objectives include the optimization of formulation parameters, evaluation of physicochemical properties, *in vitro* and *in vivo* performance assessments, and stability testing of the optimized nanomedicine. This work is expected to offer a novel strategy to minimize toxicity, enhance therapeutic efficacy, and establish *B. licheniformis* as a sustainable platform for future drug delivery systems [13].

2. MATERIALS AND METHODS

2.1 Materials: Most of the chemicals used, including Eudragit L100, Mueller–Hinton Agar, and Potassium Dihydrogen Orthophosphate, were procured from Cosmo Chem Pvt. Ltd. and Solanki Enterprises. Silver nitrate and methanol were obtained from Research Lab Fine Chem Industries and Solanki Enterprises, while Sabouraud Dextrose Agar and Triethanolamine were sourced exclusively from Solanki Enterprises.

Cell Line- L929 (Mouse Fibroblast) cells were procured from National Centre for Cell Sciences (NCCS), Pune, India and grown in Dulbecco's modified Eagles medium, DMEM (Sigma Aldrich, USA), incorporated with FBS (fetal bovine serum) and antibiotics (Penicillin and Streptomycin).

2.2 Microorganism and Culture Conditions:

The bacterial strain *Bacillus licheniformis* was isolated from soil samples were collected from rhizosphere regions of medicinal garden of Channabasweshwar Pharmacy College (Degree), Latur known for rich microbial diversity. The culture was maintained on nutrient agar slants at 4 °C and sub-cultured every two weeks to ensure viability.

2.3 Method of Preparation of Silver Nanoparticles:

Bacillus licheniformis was inoculated into nutrient broth and incubated at 37 °C for 24 h at 220 rpm. After incubation, the culture was centrifuged at 8000 × g, and the resulting supernatant was used for nanoparticle synthesis. The supernatant was mixed with silver nitrate solution (0.1 g/L or 1 mM) and kept at room temperature in the dark for 24 h, along with control flasks containing only the supernatant or only silver nitrate. The formation of silver nanoparticles was confirmed by UV–Visible spectrophotometry within the 300–700 nm wavelength range. Additionally, 5 mg of *B. licheniformis* was added to 50 mL of 1 mM silver nitrate for further synthesis. The reduction of silver ions indicated nanoparticle formation. The nanoparticles were purified by repeated centrifugation at 5000 rpm for 15 min, and the resulting pellet was collected, dried, and purified for further characterization [14].

2.4 Design of Experiments (DOE) and Quality by Design (QbD) Approach

A Quality by Design (QbD) framework was employed to systematically optimize the silver nanoparticle (AgNP) formulation variables using a Central Composite Design (CCD) within the Design-Expert® (Version 13, Stat-Ease Inc., USA) software. Two critical process parameters (CPPs) the concentration of $AgNO_3$ (A, mM) and centrifugation speed (B, rpm) were selected based on prior screening and risk assessment (Ishikawa and FMEA analysis). The critical quality attributes (CQAs) defined were particle size (nm), zeta potential (mV), and entrapment efficiency (%).

Each factor was studied at five levels ($-\alpha, -1, 0, +1, +\alpha$) with $\alpha = 1.414$. A total of 12 experimental runs (including center-point replications) were performed as per the CCD matrix to explore linear, interaction, and quadratic effects. The AgNPs were synthesized according to standardized protocol, and the resulting formulations were characterized for particle size and zeta potential using a dynamic light scattering (DLS) system (Malvern Zetasizer Nano ZS), while entrapment efficiency

was quantified by UV–visible spectroscopy after ultracentrifugation. All experiments were conducted in triplicate, and results were expressed as mean ± SD.

Table 1. Formulation Batches of Silver Nanoparticles

Std	Run	A: $AgNO_3$ (mM)	B: Centrifugation Speed (rpm)
7	1	1	7171.57
11	2	1	10000
2	3	1.5	8000
5	4	0.2929	10000
9	6	1	10000
1	7	0.5	8000
6	10	1.707	10000
3	11	0.5	12000
4	12	1.5	12000

2.5 Statistical Analysis and Optimization

A quadratic polynomial model (Eq. 1) was fitted to the data for each response:

$$Y = \beta_0 + \beta_1 A + \beta_2 B + \beta_{12} AB + \beta_{11} A^2 + \beta_{22} B^2$$

where Y is the predicted response; β terms are regression coefficients; A and B are coded independent variables. Analysis of variance (ANOVA) was used to assess model significance at $p < 0.05$. Model adequacy was evaluated by R^2, adjusted R^2, predicted R^2, Adequate Precision, and lack-of-fit tests. Response-surface and contour plots were generated to visualize variable interactions. Numerical optimization was applied using a desirability function approach to minimize particle size and maximize zeta potential magnitude and entrapment efficiency. The predicted optimal conditions were validated experimentally.

2.6 Characterization of Silver Nanoparticles

2.6.1 UV–Visible Spectroscopy: The supernatant was analyzed qualitatively using a UV–Visible spectrophotometer (Jasco V-630), with silver nitrate solution serving as the control. Spectral scanning was performed from 370 nm to 970 nm at a resolution of 1 nm. The absorption peak of AgNPs appeared between 400 nm and 470 nm, confirming nanoparticle formation through the reduction of silver nitrate [15].

2.6.2 Fourier Transform Infrared (FTIR) Spectroscopy: FTIR analysis (Model FT/IR-4600 Type A) was conducted to identify the biomolecules responsible for the stabilization and capping of AgNPs and to determine the functional groups present. Completely dried AgNP samples were used for the analysis. The spectra were recorded in the transmission range of 500–4000 cm^{-1} [16].

2.6.3 Scanning Electron Microscopy (SEM): The size and morphology of the AgNPs were examined using scanning electron microscopy (JEOL). Images were captured at different magnifications (200× and 500×). SEM analysis was used to evaluate particle morphology, surface topography, and texture of the optimized formulations [17].

2.6.4 Particle Size and Zeta Potential: The particle size, polydispersity index (PDI), and zeta potential of nanoparticles were measured using a dynamic light scattering instrument (Zetasizer). Nanoparticle suspensions were diluted with distilled water, and twelve measurements were taken to obtain average values [18].

2.6.5 Entrapment Efficiency (EE%): Entrapment efficiency was determined indirectly by centrifuging nanoparticle suspensions at 12,000 rpm for 10 min. The supernatant was mixed with Methanol and analyzed at 440 nm using UV–Visible spectrophotometry (Jasco V-630) to quantify the unentrapped drug. EE% was calculated using the formula [19]:

$$\text{EE (\%)} = \frac{(\text{Total Drug} - \text{Free Drug})}{\text{Total Drug}} \text{ X } 100$$

2.6.6 Stability Study: Formulations were stored at 40 °C/75% RH, 25 °C/65% RH, and 4 °C/55% RH for three months. Samples were analyzed monthly for drug content, percentage release, viscosity, and spreadability, and results were compared with the initial values to assess stability.

2.6.7 In Vitro Studies and Formulation of Bioinspired Nanomedicine

MTT Assay (Cytotoxicity): The cytotoxicity of PF6 was evaluated on mouse dermal fibroblast cells (L929). Cells were cultured in DMEM supplemented with 10% FBS and maintained at 37 °C in a 5% CO_2 atmosphere. Cells were seeded into 96-well plates and treated with various concentrations of PF6. After incubation, MTT reagent was added, and the resulting formazan crystals were solubilized. Absorbance was measured at 570 nm, and percentage cell viability along with IC_{50} values were calculated [20].

Wound Healing (Scratch) Assay: Mouse dermal fibroblast (L929)cells were grown to confluence on collagen-coated coverslips. A linear scratch was made using a sterile pipette tip, and detached cells were removed by washing with PBS. The remaining cells were treated with DMSO (Control), PDGF positive control, and PF6 test. After 24 h of incubation, cells were fixed, stained with DAPI, and imaged. Cell migration and wound closure were quantified using CellC software.

Antibacterial Activity: The antimicrobial activity of the synthesized nanoparticles was tested against *Escherichia coli* and *Staphylococcus aureus* using the agar well diffusion method on Mueller–Hinton and Sabouraud Dextrose Agar plates. Test samples (500 µg/mL) were loaded into wells and incubated at 37 °C for 18–24 h. Zones of inhibition were measured and compared with standard antibacterial agents [21].

3. RESULTS AND DISCUSSION

3.1 Optimization of Silver Nanoparticles Using QbD Approach

The 9 experimental runs generated particle sizes ranging from 38.27 nm to 72.14 nm, zeta potentials between –16.4 mV and –27.2 mV, and entrapment efficiencies from 71.34% to 92.14% (Table 2). This variability confirmed the influence of both $AgNO_3$ concentration and centrifugation speed on nanoparticle characteristics.

Table 2. Central Composite Design matrix with measured responses for AgNP formulations (PF1–PF9).

Std	Run	A: $AgNO_3$ (mM)	B: Centrifugation Speed (rpm)	Batch	Particle Size (nm)	Zeta Potential (mV)	Entrapment Efficiency (%)
7	1	1	7171.57	PF1	72.14	−22.0	88
11	2	1	10000	PF2	52.47	−26.0	87.14
2	3	1.5	8000	PF3	54.29	−20.2	88.11
5	4	0.2929	10000	PF4	69.89	−17.4	79.58
9	6	1	10000	PF5	49.21	−16.4	78.24
1	7	0.5	8000	**PF6**	**38.27**	**−27.2**	**92.14**
6	10	1.707	10000	PF7	40.24	−24.4	77.88
3	11	0.5	12000	PF8	53.6	−25.4	71.34
4	12	1.5	12000	PF9	48.56	−26.8	74.12

3.2 ANOVA and Model Fitting

The quadratic models were found statistically significant ($p < 0.05$) for all responses. The regression analysis revealed strong correlation coefficients ($R^2 > 0.90$), validating model adequacy.

Then include subsections for each:

Particle Size: The quadratic model ($F = 11.21$, $p = 0.0371$; $R^2 = 0.9492$) indicated that both *$AgNO_3$ concentration* (A) and *centrifugation speed* (B) significantly affected particle size. Increasing $AgNO_3$ enlarged the particles, while higher

centrifugation reduced them.

Equation:

Particle Size = $38.27 - 5.21A - 5.68B + 6.02AB + 5.40A^2 + 11.38B^2$

Zeta Potential: The linear model ($F = 5.64$, $p = 0.0419$; $R^2 = 0.6528$) showed that centrifugation speed (B) had a significant negative correlation, yielding more negative values (improved stability).

Equation:

Zeta Potential = $-22.87 + 0.03A - 3.29B$

Entrapment Efficiency: The quadratic model ($F = 12.83$, $p = 0.0308$; $R^2 = 0.9553$) indicated that both $AgNO_3$ concentration (A) and centrifugation speed (B^2) were significant. Optimal entrapment occurred near 0.5 mM $AgNO_3$ and 8000–10000 rpm.

Equation:

Entrapment Efficiency = $92.14 - 5.00A - 1.94B - 1.51AB - 4.26A^2 - 7.33B^2$

3.3 Response Surface and Optimization

Response surface plots (Figure 1A–C) illustrate the interactive effects of $AgNO_3$ concentration and centrifugation speed on nanoparticle size, zeta potential, and entrapment efficiency. The optimal formulation (PF6) yielded a particle size of 38.27 nm, zeta potential of −27.2 mV, and entrapment efficiency of 92.14%. Experimental validation confirmed model predictability within <5% deviation.

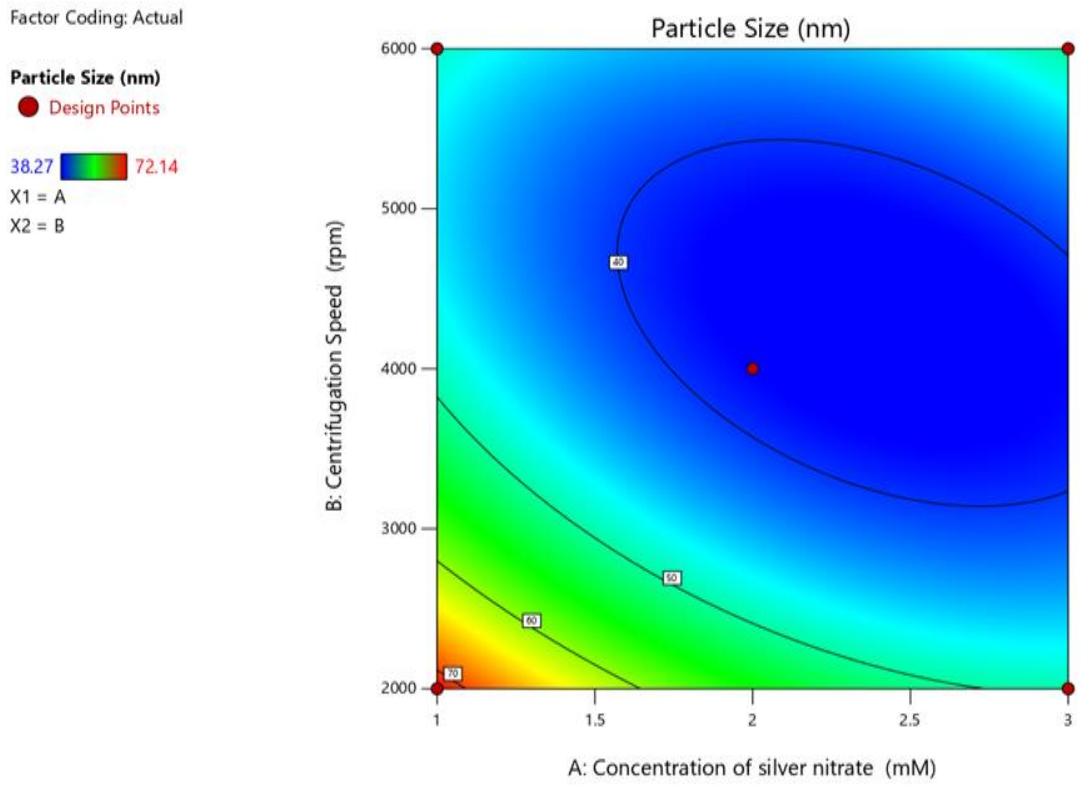

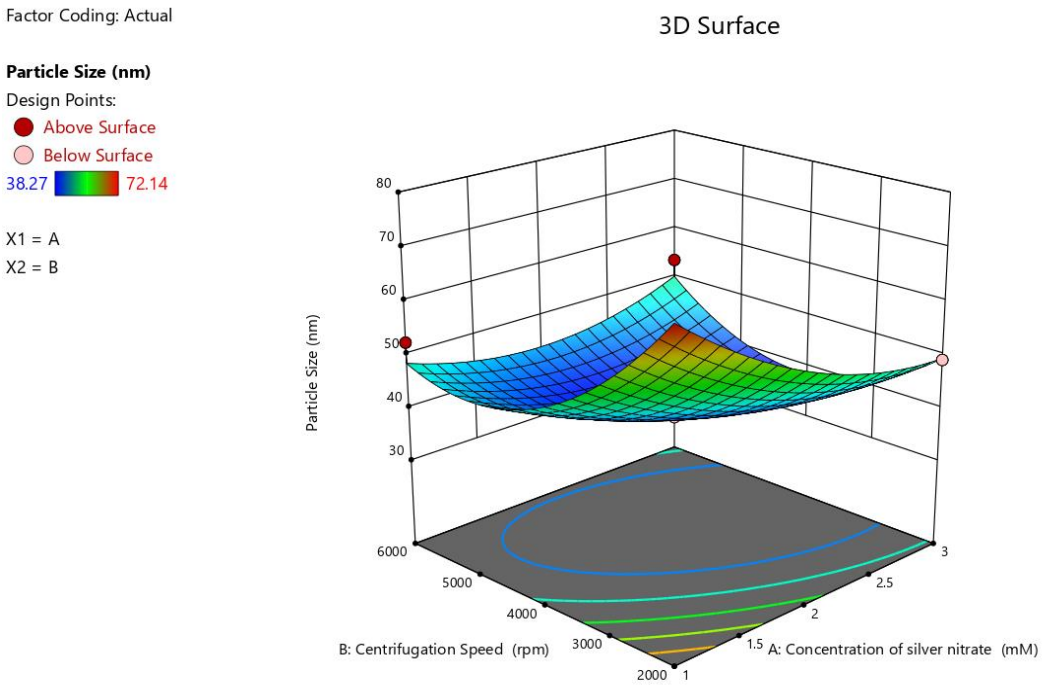

Figure 1. 3D Surface Plot for particle Size with desirability overlay

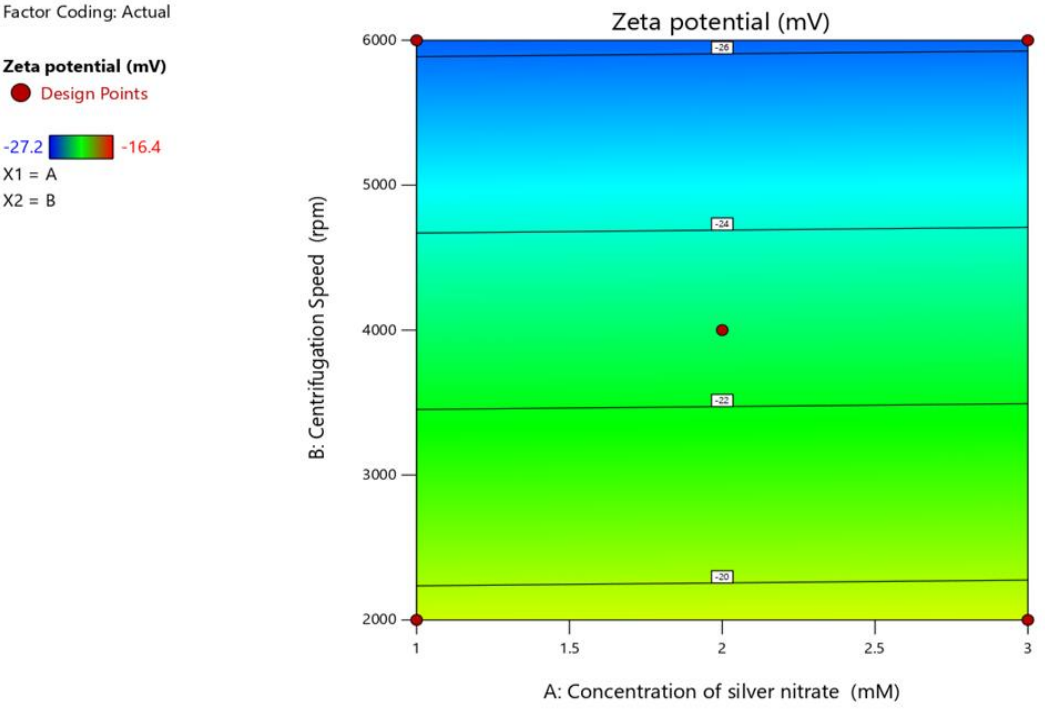

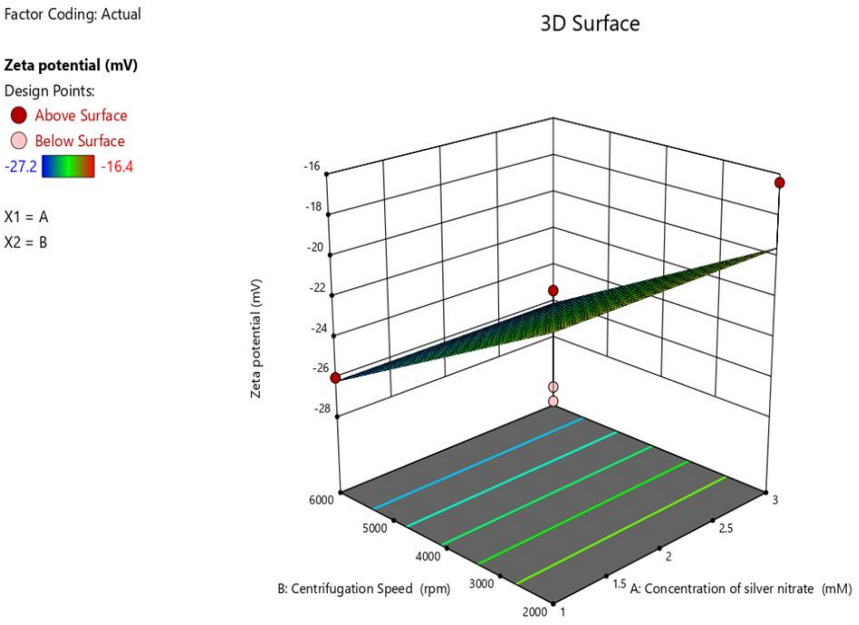

Figure 2. 3D Response surface for Zeta Potential with desirability overlay

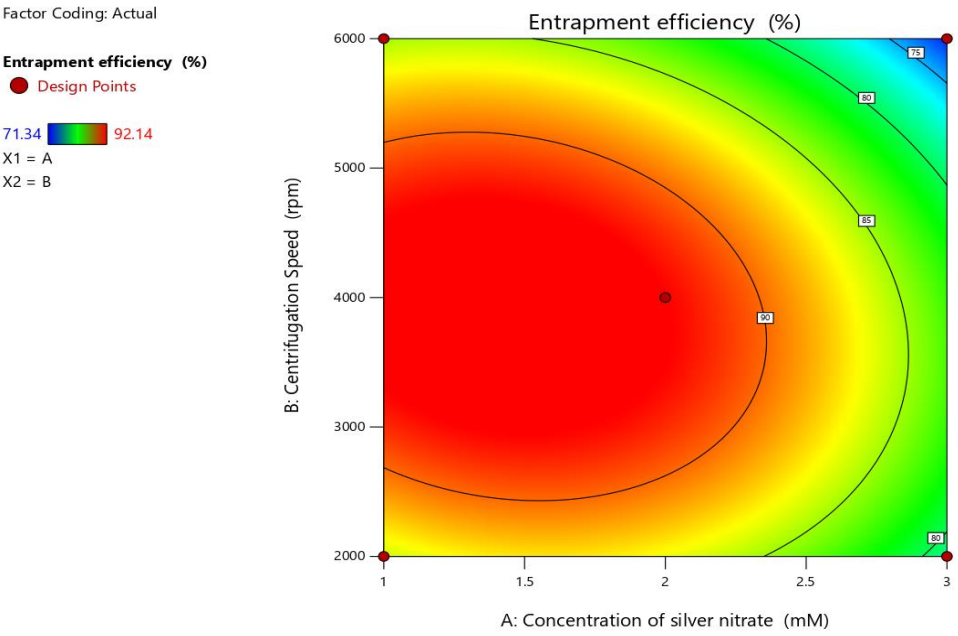

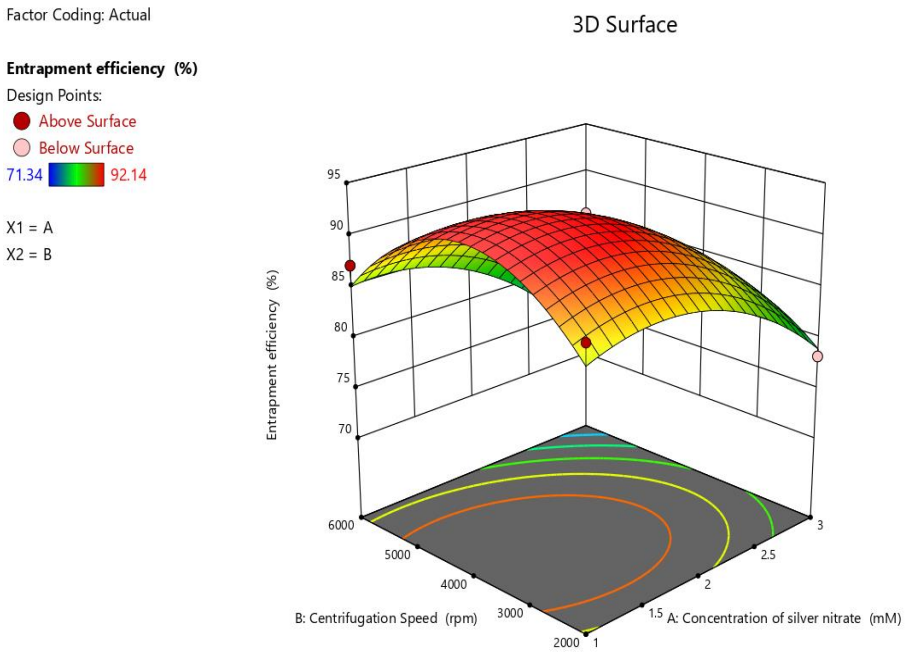

Figure 3. Response surface for Entrapment Efficiency with desirability overlay

3.4 Characterization of Optimized Silver Nanoparticles

3.4.1 UV–Visible Spectroscopy: The UV–visible absorption spectrum of PF6 displayed a distinct surface plasmon resonance (SPR) peak at 416 nm, confirming nanoparticle formation via reduction of Ag^{+} ions by *B. licheniformis* biomolecules.

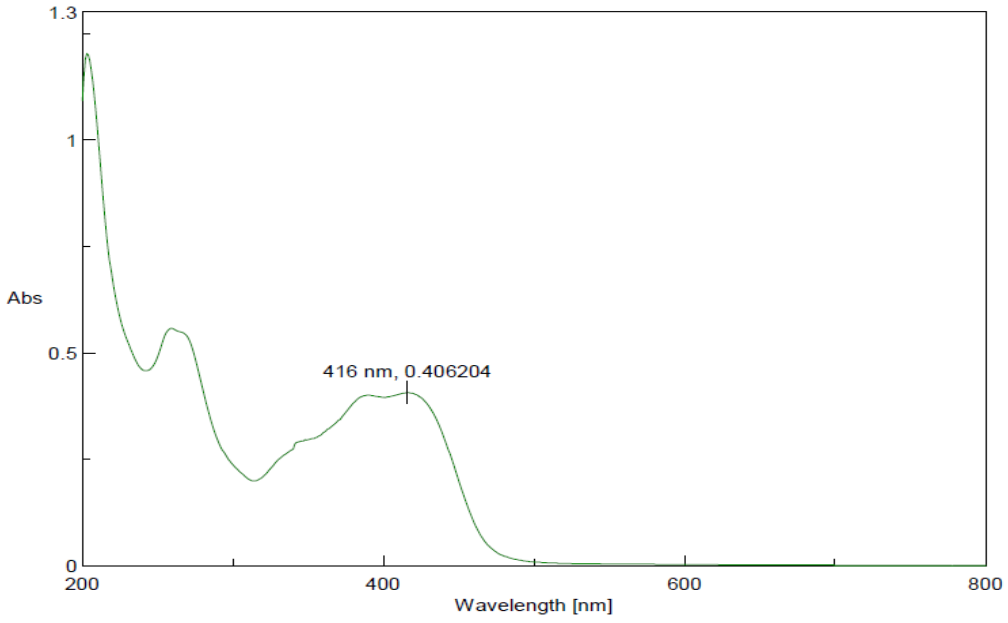

Figure 4. UV–Visible absorption spectrum of optimized AgNP formulation (PF6).

3.4.2 Fourier Transform Infrared (FTIR) Analysis: The FTIR spectra revealed peaks at 3425 cm^{-1} (O–H stretch), 1637 cm^{-1} (C=O stretch), and 1056 cm^{-1} (C–O–C stretch), indicating the presence of proteins, phenolic compounds, and other functional groups that stabilized and capped the nanoparticles.

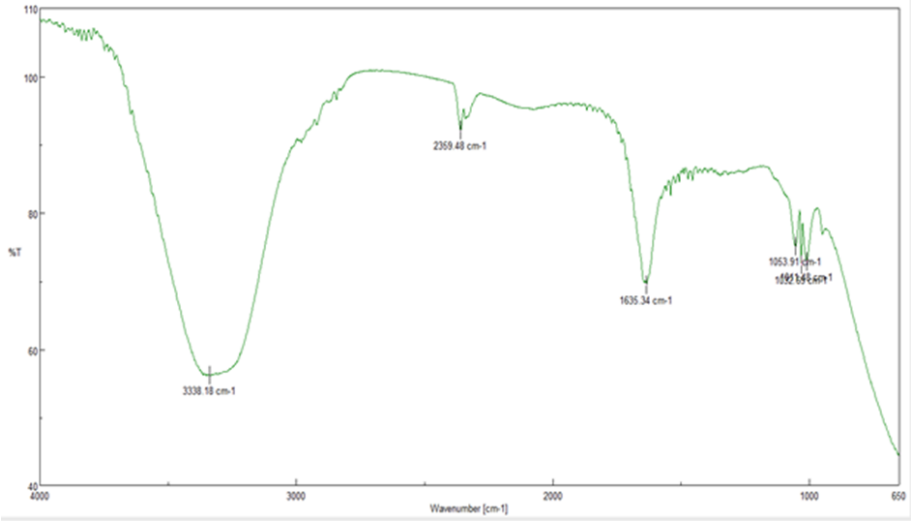

Figure 5. FTIR spectrum of optimized AgNPs (PF6).

3.4.3 Scanning Electron Microscopy (SEM): SEM micrographs (Figure 4) revealed predominantly spherical, irregularly dispersed nanoparticles with sizes below 50 nm. The rough surface morphology suggests bioorganic coating, which enhances dispersion stability.

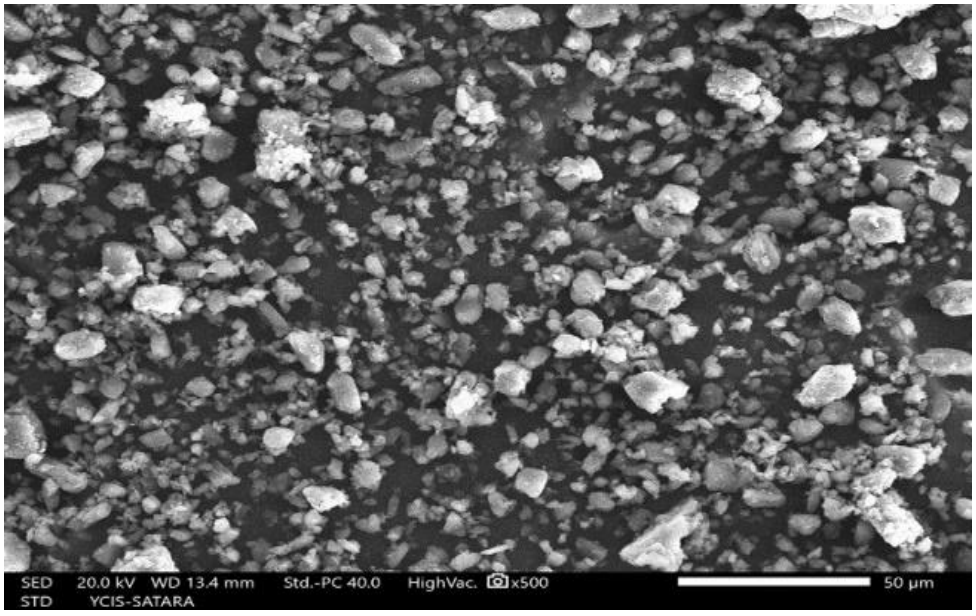

Figure 6. SEM images of optimized AgNPs (PF6) at 200× and 500× magnification.

3.4.4 Particle Size, Zeta Potential, and Entrapment Efficiency: Among all formulations, PF6 exhibited the most desirable physicochemical profile 38.27 nm, –27.2 mV, and 92.14% EE. The high negative zeta potential indicates strong electrostatic stabilization, while small particle size ensures enhanced cellular uptake and controlled release.

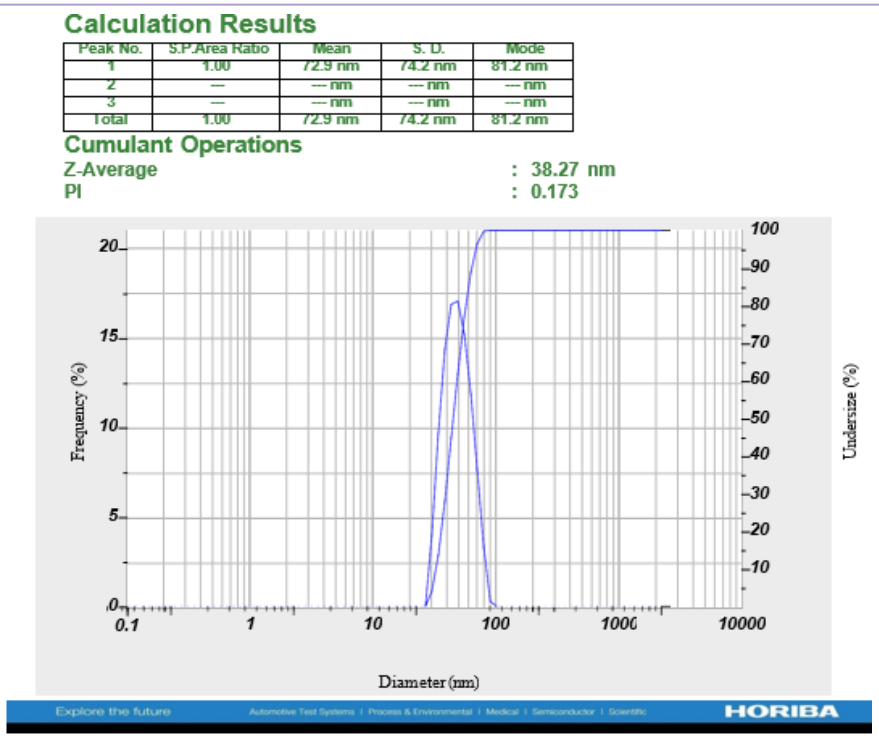

Figure 7. Particle size of optimized batch PF6

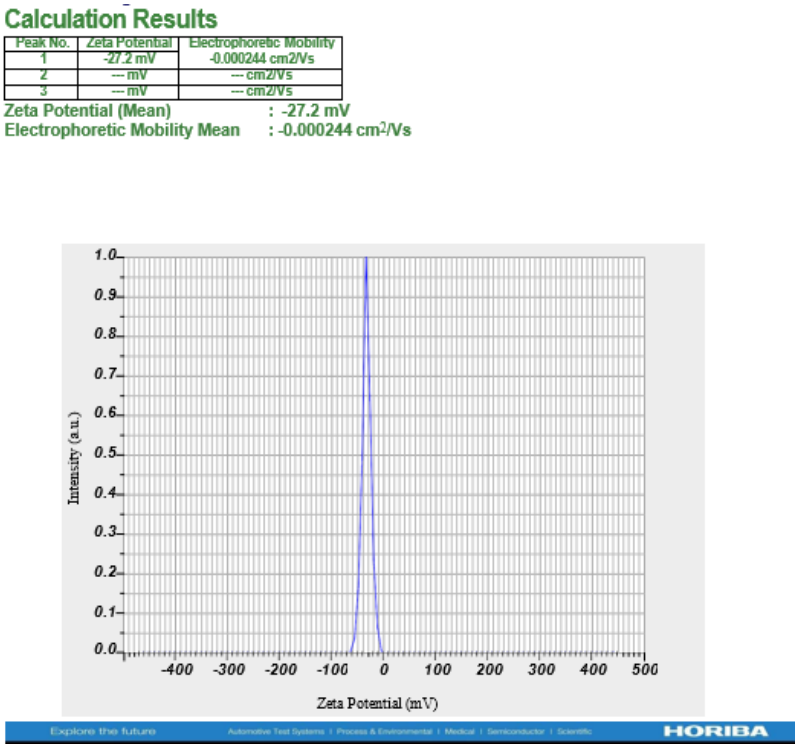

Figure 8. Zeta Potential of optimized batch PF6

3.5 Stability Studies: The PF6 formulation maintained excellent stability over three months at varied storage conditions (4°C, 25°C ±2°C, and 40°C/75% RH). Particle size, PDI, and entrapment efficiency showed negligible variations (≤1%), confirming no aggregation, leakage, or phase separation. These results demonstrate robust formulation stability, ensuring sustained shelf life and reproducibility.

Table 3. Effect of storage conditions on physicochemical stability of optimized AgNPs (PF6).

Time Period	Condition	Particle size	Drug entrapment	PDI
Initial	—	121.8	74.11	0.296
One Month	RT (25°C±2°C)	121.8	74.11	0.296
	40°C/75% RH	121.5	74.11	0.295
	4°C ± 1°C	121.5	74.08	0.295
Two Months	RT (25°C±2°C)	121.4	74.08	0.293
	40°C/75% RH	121.3	74.04	0.293
	4°C ± 1°C	121.3	74.03	0.292
Three Months	RT (25°C±2°C)	121.1	74.03	0.292
	40°C/75% RH	121.1	74.02	0.29
	4°C ± 1°C	120.9	74.02	0.29

3.6 In Vitro Biological Evaluation

3.6.1 Cytotoxicity (MTT Assay): The MTT assay on fibroblast cells demonstrated that PF6 retained biocompatibility at lower concentrations while exhibiting dose-dependent cytotoxicity. Cell viability decreased from 90.93% at 0.5 µL/mL to 35.45% at 100 µL/mL, with an IC_{50} value of 35.63 µL/mL. These findings indicate controlled cytotoxic effects suitable for therapeutic applications without compromising cellular integrity at optimized doses.

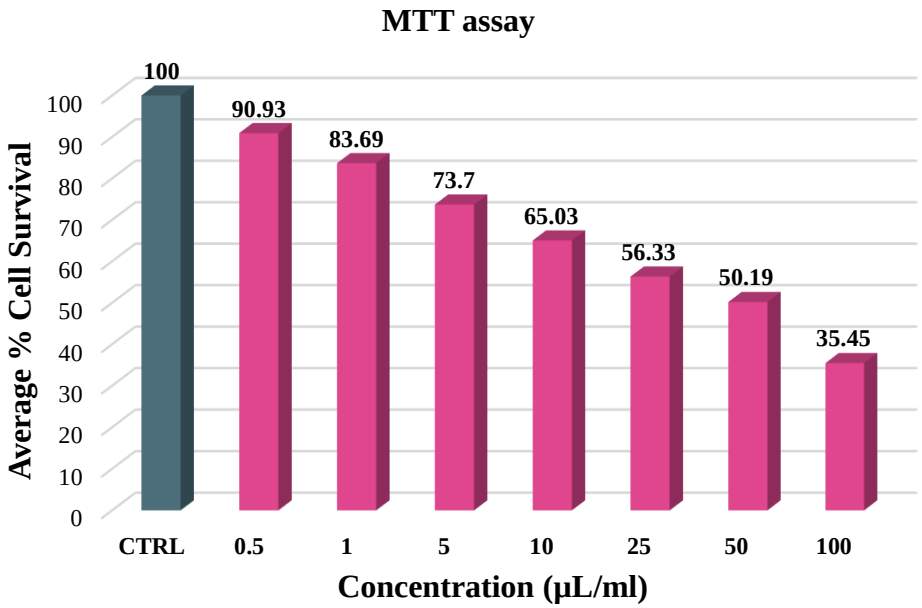

Figure 5. Dose–response curve for PF6 cytotoxicity (MTT assay).

3.6.2 Wound Healing (Scratch) Assay: The PF6 formulation significantly enhanced fibroblast migration in a dose-dependent manner. At 50 µg/mL, PF6 achieved 58.5% wound closure, closely approaching the positive control PDGF (67.8%). Even at lower concentrations (0.5–10 µg/mL), PF6 accelerated closure by 1.5-2.4-fold compared to control, indicating strong pro-migratory and regenerative potential. These outcomes suggest that the phytoconstituent-loaded emulsomes facilitate tissue repair and could be valuable for respiratory epithelium regeneration in cystic fibrosis.

Table 4. Effect of Test Compounds on Fibroblast Migration in Scratch Wound Healing Assay			
Treatment	**Concentration**	**Mean % Wound Closure ± SD**	**Relative Migration (vs. Control)**
Control (DMSO)	0.25%	20.4 ± 2.1%	1.00
PDGF (Positive Control)	2 ng/ml	67.8 ± 3.5%	3.32
Pf6	0.25 µg/ml	19.3 ± 2.7%	0.42
Pf6	0.5 µg/ml	28.1 ± 3.1%	1.05
Pf6	1 µg/ml	37.6 ± 2.3%	1.82
Pf6	10 µg/ml	42.8 ± 2.4%	2.10
Pf6	50 µg/ml	58.5 ± 3.0%	2.87

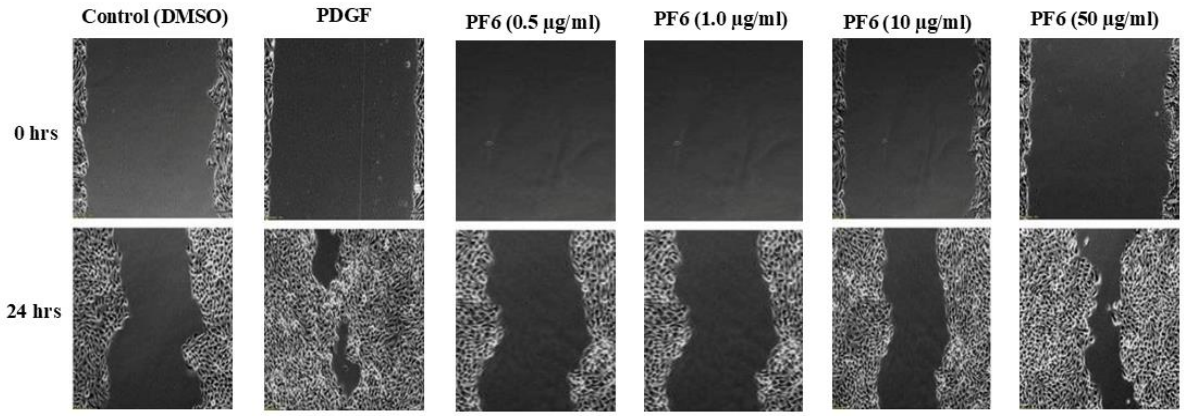

Figure 6. Microscopic images of scratch assay showing dose-dependent wound closure by PF6.

3.6.3 Antibacterial Activity: The optimized batch PF6 demonstrated notable antibacterial activity against E. coli (18.81 mm) and S. aureus (18.77 mm) compared to the standard Streptomycin (22.62 mm and 21.65 mm, respectively). The absence of inhibition in the control (DMSO) validates the intrinsic antibacterial property of the extract. These findings support the broad-spectrum antimicrobial potential of the formulation, relevant to cystic fibrosis–associated lung infections.

Table 5. Antibacterial activity of PF6 compared with standard antibiotics			
Sr.no	**Sample Name**	**Zone of Inhibition (mm)**	
		E-Coli	***Staphylococcus aureus***
1	Control (DMSO)	NA	NA
2	Standard (**Streptomycin**)	22.62 mm	21.65 mm
3	Optimized Batch (PF6)	18.81 mm	18.77 mm

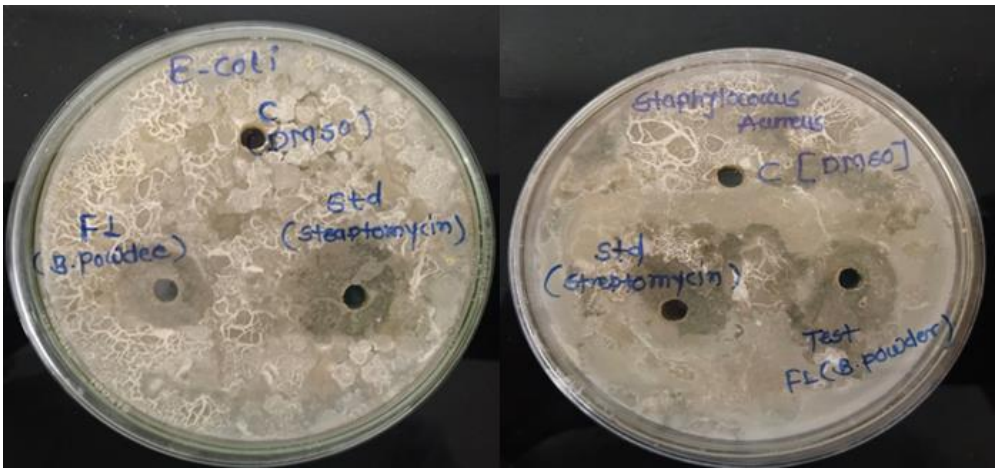

Figure 7. Zones of inhibition produced by PF6 against *E. coli* and *S. aureus*.

4. CONCLUSION AND FUTURE PERSPECTIVES

This study demonstrated the successful green synthesis of silver nanoparticles (AgNPs) using Bacillus licheniformis as a natural nanofactory. The Quality by Design (QbD) approach optimized formulation parameters to produce stable, biocompatible nanoparticles with a particle size of 38.27 nm, zeta potential of -27.2 mV, and 92.14% entrapment efficiency. Spectroscopic and microscopic analyses confirmed well-dispersed, bio-capped nanoparticles with excellent stability.

Biological evaluations revealed that the optimized PF6 formulation significantly enhanced fibroblast migration and wound closure while showing potent antibacterial activity against E. coli and S. aureus. These findings highlight the dual wound-healing and antimicrobial efficacy of bioinspired AgNPs.

Future Perspectives.

Further studies should explore the molecular mechanisms and in vivo efficacy of these nanoparticles. Integrating B. licheniformis derived AgNPs into advanced delivery systems such as hydrogels or nanofiber scaffolds could improve therapeutic performance and clinical translation. Overall, this eco-friendly nanotechnology offers a promising platform for next-generation regenerative and antimicrobial therapies

REFERENCES

[1] Bayda S, Adeel M, Tuccinardi T, Cordani M, Rizzolio F. The history of nanoscience and nanotechnology: from chemical–physical applications to nanomedicine. Molecules. 2019;25(1):112.

[2] Paramasivam G, Dhanasekaran S, Kalpana D, Mohan R. Nanomaterials – synthesis, characterization, recent advances and applications: A review. J King Saud Univ Sci. 2021;33(2):101322.

[3] Su CH, Chiu HC, Chen CW. Advances in nanotechnology-based strategies for breast cancer therapy: from diagnosis to treatment. Cancers (Basel). 2020;12(3):731.

[4] Joudeh N, Linke D. Nanoparticle classification, physicochemical properties, characterization, and applications: a comprehensive review for biologists. J Nanobiotechnology. 2022;20(1):262.

[5] Chavali MS, Nikolova MP. Metal oxide nanoparticles and their applications in nanotechnology. SN Appl Sci. 2019;1(6):607.

[6] Mohammed-Sadhakathullah A, Alzahrani S, Alharbi SA, Abdulhakeem BH, Ameen F. Recent advancements and biological prospects of organic nanoparticles in drug delivery systems: a comprehensive review. Biomed Pharmacother. 2023;162:114637.

[7] Rudrapal M, Khan J, Alshammari TM, Althagafi S, Srivastava S, Khairnar SJ, et al. Carbon-based nanomaterials: promising platforms for cancer theranostics. Molecules. 2022;27(10):3132.

[8] Ozyurt D, Tekinay AB, Dana A. Carbon nanodots for biomedical and optoelectronic applications: a review of recent advances. Nanomaterials (Basel). 2023;13(1):75.

[9] Pirzada M, Altintas Z. Nanomaterials for healthcare biosensing applications. Sensors (Basel). 2019;19(23):5311.

[10] Laroui H, Dalmasso G, Yan Y, Nguyen HT, Sitaraman SV, Merlin D. Drug-loaded nanoparticles targeted to the colon with polysaccharide hydrogel reduce colitis in a mouse model. Gastroenterology. 2013;145(3): 500–

511.e3.

[11] Kalimuthu, K., et al. Extracellular biosynthesis of gold nanoparticles by Bacillus licheniformis. Materials Letters. 2008;62(29):4411–4413.

[12] Sunkar, S., Nachiyar, C. V. Microbial synthesis and characterization of silver nanoparticles by Bacillus licheniformis. Colloids and Surfaces B: Biointerfaces. 2010;77(2):291–295.

[13] Goudarzi, M., et al. Antimicrobial and antibiofilm activities of lipopeptides from Bacillus licheniformis: Promising agents in nanomedicine. Pharmaceutics. 2023;15(7):1893.

[14] Adlin J, Gowthamarajan K, Somashekhara C. Formulation and evaluation of nanoparticles containing flutamide. Int J ChemTech Res. 2009;1(4):1331-34.

[15] Uday TC, Shivabasappa PM, Sanjay SS, Maruti MS. Development and Validation of Stability Indicating UV-spectrophotometric Method for the simultaneous estimation of telmisartan and metformin hydrochloride in bulk drugs. IJPER. 2021;55(2):590-7. doi: 10.5530/ijper.55.2.98. Uday TC, Shivabasappa PM, Sanjay SS, Maruti MS. Development and Validation of Stability Indicating UV-spectrophotometric Method for the simultaneous estimation of telmisartan and metformin hydrochloride in bulk drugs. IJPER. 2021;55(2):590-7. doi: 10.5530/ijper.55.2.98.

[16] Maaben S, Schwarz C, Mehnert W, Lucks JS, Yunis-Specht F, Muller BW, Muller RH. Comparison of cytotoxicity between polyester nanoparticles and solid lipid nanoparticles. InProc Int Symp Control Rel Bioact Mater 1993 (Vol. 20, pp. 490-491).

[17] Karuppusamy C, Venkatesan P. Preformulation Parameters Characterization to Design, Development and Formulation of Miglitol Loaded Nanoparticles. Journal of Pharmaceutical Sciences and Research. 2017 Mar 1;9(3):326.

[18] Das S, Banerjee R, Bellare J. Aspirin loaded albumin nanoparticles by coacervation: implications in drug delivery. Trends in Biomaterials and Artificial Organs. 2005 Jan 1;18(2):203-13.

[19] Kumar V, Sharma N, Maitra SS. In vitro and in vivo toxicity assessment of nanoparticles. International Nano Letters. 2017 Dec;7(4):243-56.

[20] Elsayed SI, Girgis GN, El-Dahan MS. Formulation and evaluation of Pravastatin sodium-loaded PLGA nanoparticles: in vitro–in vivo studies assessment. International Journal of Nanomedicine. 2023 Dec 31:721-42.

[21] Salem HF, Eid KA, Sharaf MA. Formulation and evaluation of silver nanoparticles as antibacterial and antifungal agents with a minimal cytotoxic effect. Int. J. Drug Deliv. 2011 Apr 1;3(2):293-304.